7-2006

Steady-Periodic Green's Functions and Thermal-Measurement Applications in Rectangular Coordinates

Kevin . D. Cole
University of Nebraska - Lincoln, kcole1@unl.edu

Steady-Periodic Green's Functions and Thermal-Measurement Applications in Rectangular Coordinates

Kevin D. Cole
Mechanical Engineering Department,
University of Nebraska–Lincoln,
Lincoln, NE 68588-0656
e-mail: kcole1@unl.edu

Methods of thermal property measurements based on steady-periodic heating are indirect techniques, in which the thermal properties are deduced from a systematic comparison between experimental data and heat-transfer theory. In this paper heat-transfer theory is presented for a variety of two-dimensional geometries applicable to steady-periodic thermal-property techniques. The method of Green's functions is used to systematically treat rectangles, slabs (two dimensional), and semi-infinite bodies. Several boundary conditions are treated, including convection and boundaries containing a thin, high-conductivity film. The family of solutions presented here provides an opportunity for verification of numerical results by the use of distinct, but similar, geometries. A second opportunity for verification arises from alternate forms of the Green's function, from which alternate series expressions may be constructed for the same unique temperature solution. Numerical examples are given to demonstrate both verification techniques for the steady-periodic response to a heated strip. [DOI: 10.1115/1.2194040]

Keywords: heat conduction, thin film, thermal wave, pulse heating, thermal properties

1 Introduction

Steady-periodic heat conduction, of interest for thermal-property measurements, may be treated analytically in two ways. In the time-domain approach, the solution can be stated with the Duhamel integral as a time convolution between the heating history and the step response [1]. A particular simplification is possible if the time history of the heating has a simple wave shape (on-off, sawtooth, etc.). In these cases the convolution integral can be evaluated in closed form so that the time dependence reduces to a series involving decaying time exponentials. This approach is used for determination of thermal properties by the thermal hot-strip method [2–5].

The frequency-domain approach is appropriate if the heating history is sinusoidal [6], or, if the heating is simply periodic and a phase-locked amplifier is used to select the response at the periodic frequency. This is the approach used for thermal-property measurements by photothermal techniques [7,8]. In a unique study, Aviles-Ramos [9] applied the frequency-domain approach to virtual steady-periodic data which was constructed, via Fourier series, from transient non-periodic data.

The frequency-domain approach has also been applied to the 3-omega method for determination of thermal properties [10]. In this method a metallic strip is plated on the sample, and suitable electronics are used to periodically energize the strip and simultaneously measure its temperature response. The temperature response is systematically compared with theory to deduce the thermal properties of the sample. The 3-omega method has recently been extended to two-dimensional layered composite materials [11,12] with a matrix technique originally described by Carlaw and Jaeger [1] for one-dimensional materials. In this method a matrix equation, constructed from matching conditions between adjacent layers, is solved to satisfy all the inter-layer boundary conditions simultaneously. In the traditional matrix technique, steady-periodic heating is applied to one surface of the composite and no internal heating of the material is considered. In contrast, the Green's function (GF) method allows for internal heating, such as from optical absorption within partially transparent layers. In previous work by the author, the Green's function method was combined with the matrix technique for one-dimensional heat transfer in a layered material [13] and for a layered material heated by an axisymmetric laser beam [14].

The purpose of this paper is to revisit steady-periodic heat conduction with the method of Green's functions (GFs). The GF approach provides a comprehensive set of solutions and specific strategies for improving the numerical evaluation of these solutions. The geometries under discussion, two-dimensional bodies with planar boundaries in the Cartesian coordinate system, have practical application to thermal property measurements.

There are several recent books on Green's functions applied to heat conduction. Beck et al. [15] give a large number of GFs for transient heat conduction. Both GF and temperature solutions are organized according to a numbering system for the domain shape and for the kind of boundary conditions present. Five kinds of boundary conditions are discussed. Although several two-dimensional geometries are discussed, no steady-periodic cases are given. Duffy [16] gives a large number of GFs for several differential equations. There is a section devoted to steady heat conduction (Poisson equation) in two-dimensional rectangular geometries, and boundaries of kinds 1, 2, and 3 are given. However, no two-dimensional transient solutions are treated. Sheremet [17] discusses GFs for the Lamé and Poisson equations in rectangular coordinates. Several GFs for steady two-dimensional heat conduction are given, however only boundaries of kinds 1 and 2 are treated. Mandelis [18] is devoted exclusively to steady-periodic heat conduction with the method of GF, and solutions are given for a variety of geometries and boundary conditions of types 1, 2 or 3. Although many cases are given in Cartesian coordinates, the emphasis is on one- and three-dimensional cases; only one GF is given that is two-dimensional in Cartesian coordinates.

The contributions of this paper are threefold. First, a great many

Contributed by the Heat Transfer Division of ASME for publication in the JOURNAL OF HEAT TRANSFER. Manuscript received June 6, 2005; final manuscript received November 28, 2005. Review conducted by A. Haji-Sheikh. Paper presented at the 2005 ASME International Mechanical Engineering Congress (IMECE2005), November 5–11, 2005, Orlando, Florida.

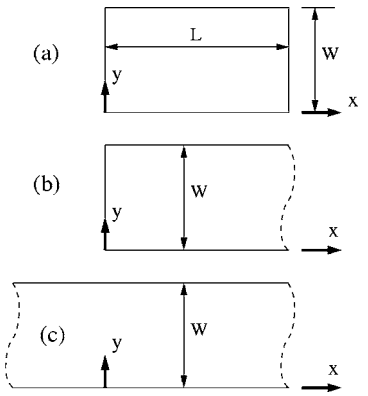

Fig. 1 Geometries under discussion include (*a*) rectangles, (*b*) semislabs, and (*c*) slabs

steady-periodic solutions are presented systematically with the method of GFs for rectangles, slabs, semislabs, and semi-infinite regions. All solutions presented are two dimensional. Second, five kinds of boundary conditions are treated in a unified fashion: specified temperature; specified heat flux; specified convection; a high-conductivity surface film; and a high-conductivity surface film with convection. To the author's knowledge many of the surface-film solutions for steady-periodic conduction have not been published before. Third, alternate forms of the GFs are given for several geometries, which provide for efficient numerical computation and allow for independent verification that the numerical results are correct.

The paper is divided into sections on temperature, Green's functions, measurement applications, and numerical examples. In the next section the temperature solution is given for a wide variety of body shapes in rectangular coordinates.

2 Temperature in Rectangular Coordinates

Consider the temperature in a two-dimensional domain in rectangular coordinates. The temperature distribution $\tilde{T}(x,y,t)$ satisfies

$$\frac{\partial^2\tilde{T}}{\partial x^2}+\frac{\partial^2\tilde{T}}{\partial y^2}-\frac{1}{\alpha}\frac{\partial\tilde{T}}{\partial t}=-\frac{1}{k}\tilde{g}(x,y,t) \quad \text{in domain } \Omega \tag{1}$$

$$k_i\frac{\partial\tilde{T}}{\partial n_i}+h_i\tilde{T}+(\rho cb)_i\frac{\partial\tilde{T}}{\partial t}=\tilde{f}_i(x_i,y_i,t); \quad \text{at boundary } i \tag{2}$$

Domain Ω can include the rectangle, semislab and slab as shown in Fig. 1. Additional geometries included in Ω but not shown in Fig. 1 are the semi-infinite body ($0<y<\infty$) and the infinite body.

Index i represents the physical boundaries, up to a maximum of four boundaries, for body shapes considered here. The boundary condition may be one of five kinds at each boundary depending on the values of coefficients k_i, h_i, and b_i (refer to Table 1): boundary type 1 is specified temperature; boundary type 2 is specified heat flux; boundary type 3 is specified convection; boundary type 4 is specified heat flux and a surface film of thickness b_i; and boundary type 5 is specified convection and a surface film. Boundary type 0 is also used to represent a boundary at infinity.

Since in this paper the applications are limited to steady-periodic heating, we take the heating terms $\tilde{g}$ and $\tilde{f}$ and the resulting temperature $\tilde{T}(x,y,t)$ to be steady periodic at a single frequency. That is, let

$$\tilde{g}(x,y,t)=\text{Real}[g(x,y,\omega)e^{j\omega t}]$$

$$\tilde{f}_i(x_i,y_i,t)=\text{Real}[f_i(x_i,y_i,\omega)e^{j\omega t}] \tag{3}$$

Table 1 Boundary conditions for temperature

Number	Description	Boundary condition
0	Boundary at ∞	($\partial\tilde{T}$ bounded)
1	Specified temperature	$\tilde{T}=\tilde{f}_i$
2	Specified heat flux	$k\partial\tilde{T}/\partial n_i=\tilde{f}_i$
3	Convection	$k\partial\tilde{T}/\partial n_i+h_i\tilde{T}=\tilde{f}_i$
4	Heat flux and surface film	$k\frac{\partial\tilde{T}}{\partial n_i}+(\rho cb)_i\frac{\partial\tilde{T}}{\partial t}=\tilde{f}_i$
5	Convection and surface film	(see Eq. (2))

$$\tilde{T}(x,y,t)=\text{Real}[T(x,y,\omega)e^{j\omega t}]$$

Now in Eqs. (1) and (2) replace $\tilde{g}$, $\tilde{f}_i$, and $\tilde{T}$ with $ge^{j\omega t}$, $f_ie^{j\omega t}$, and $Te^{j\omega t}$, respectively, to find the steady-periodic heat conduction equation

$$\frac{\partial^2T}{\partial x^2}+\frac{\partial^2T}{\partial y^2}-\frac{j\omega}{\alpha}T=-\frac{1}{k}g(x,y,\omega); \quad \text{in domain } \Omega \tag{4}$$

$$k_i\frac{\partial T}{\partial n_i}+[h_i+j\omega(\rho cb)_i]T=f_i(x_i,y_i,\omega); \quad \text{at boundary } i \tag{5}$$

In this paper complex-valued $T(x,y,\omega)$ is interpreted as the steady-periodic temperature (Kelvin) at a single frequency ω. For further discussion of this point see [18]. Later in the paper, results will be discussed in the form of amplitude and phase of this temperature.

The steady-periodic temperature will be found with the Green's function (GF) method. Assume for the moment that the appropriate GF in frequency space, G, is known. Then the steady-periodic temperature is given by the following integral equation (see [15])

$$T(x,y,\omega)=\frac{\alpha}{k}\int\int g(x',y',\omega)G(x,x',y,y',\omega)dx'dy' \quad \text{(for volume heating)}$$

$$+\alpha\int_{s_i}f_i\times\begin{bmatrix}-\partial G/\partial n_i' & \text{(type 1 only)}\\ \frac{1}{k}G & \text{(type 2 – 5)}\end{bmatrix}ds_i' \quad \text{(at boundaries)} \tag{6}$$

Note that the same GF appears in each integral term but it is evaluated at locations appropriate for each integral.

3 Green's Function

The GF represents the response at (x,y) to a steady-periodic point source of heat located at (x',y'). The GF associated with Eqs. (4)–(6) is defined by

$$\frac{\partial^2G}{\partial x^2}+\frac{\partial^2G}{\partial y^2}-\frac{j\omega}{\alpha}G=-\frac{1}{\alpha}\delta(x-x')\delta(y-y') \quad \text{in domain } \Omega \tag{7}$$

$$k_i\frac{\partial G}{\partial n_i}+[h_i+j\omega(\rho cb)_i]G=0; \quad \text{at boundary } i \tag{8}$$

Here $\delta(\cdot)$ is the Dirac delta function. It is important to note that the GF satisfies homogeneous boundary conditions of the same kind as the temperature equation.

Table 2 Eigenfunctions for rectangles, slabs, and semislabs

Case	$Y_n(y)$
Y11, Y12, Y13, Y14, and Y15 Y21, Y22, Y23, Y24, and Y25 YK1, YK2, YK3, YK4, and YK5[a]	$\sin(\gamma_n y)$ $\cos(\gamma_n y)$ $\gamma_n W\cos(\gamma_n y)$ $+(\lambda_1 W/k)\sin(\gamma_n y)$

[a]K=3, 4, or 5

4 GF Number

The GF needed for a given temperature solution is determined by the body shape and by the kind of boundary conditions present. To distinguish among all the different GFs that are included in this paper, we use a "number" of the form *XijYkl* in which *X* and *Y* represent the coordinate axes, and the letters following each axis name take on values 1, 2, 3, 4, or 5 to represent the kind of boundary conditions present at the body faces normal to that axis. Number 0 is also used to represent a boundary at infinity.

For example, number *X*12 represents boundary conditions of type 1 at $x=0$ and type 2 at $x=L$, and *X*30 represents boundary conditions of type 3 at $x=0$ on a body that extends to $x=\infty$. As another example, number *X*11*Y*13 describes a GF for a rectangle with three faces having type 1 boundaries ($G=0$) and the face at $y=W$ has a type 3 boundary (convection). As a final example, number *X*00*Y*12 represents a slab, infinite in the x direction, with boundary of type 1 at $y=0$ and a boundary of type 2 at $y=W$.

The number system described here is useful for classifying Green's functions. Extensions of this number system for classifying temperature solutions, including designations for energy generation, initial conditions, and time and space distributions in the boundary conditions, are given in the book by Beck et al. [15] and in the Green's Function Library, an internet site devoted to Green's functions [19].

5 GF for the Rectangle, Semislab, and Slab

The GF may be found as a series expansion involving eigenfunctions for bodies of finite size in at least one direction. This applies to rectangles, semislabs and slabs in rectangular coordinates in two dimensions. The GFs for these body shapes that satisfy Eqs. (7) and (8) are given below in a single-sum form

$$G(x,y,\omega|x',y') = \sum_{n=0}^{\infty} \frac{Y_n(y)Y_n^*(y')}{N_y(\gamma_n)} P(x,x',\sigma) \tag{9}$$

The series for the GF contains eigenfunction Y_n, norm N_y, and kernel function P which will be discussed below. The $n=0$ term is needed only when zero is an eigenvalue (when *Y*22 is part of the GF number).

5.1 Eigenfunctions. The y-direction eigenfunction satisfies the following ordinary differential equation

$$Y_n''(y) + \gamma_n^2 Y_n(y) = 0, \quad (0 < y < W) \tag{10}$$

where γ_n is the associated eigenvalue. There are three different eigenfunctions associated with the 25 possible combinations of boundary condition *YKL* ($K,L=1, 2, 3, 4,$ or 5). Eigenfunctions $Y_n(y)$ are composed of sines and cosines, and are listed in Table 2. Table 3 contains the associated inverse norms and eigenconditions (or eigenvalues for simple cases). For case Y22 the eigenvalue may also take on the value zero.

Boundary conditions of type 4 or 5, which include a thin surface film, require special care because the eigenvalues are complex numbers and the eigenfunctions contain complex-valued sine and/or cosine. Complex-valued eigenvalues have been previously shown to occur for heat conduction in multi-layer, multi-dimensional bodies [20].

Table 3 Inverse norm and eigenvalues or eigencondition. Note $B_i=\lambda_i W/k$.

Case	$N(\gamma_n)^{-1}$	γ_n or eigencondition
*Y*11	$2/W$	$n\pi/W$
*Y*12	$2/W$	$(2n-1)\pi/(2W)$
*Y*13, *Y*14, Y15[a]	$2\phi_{2n}/W$	$\gamma_n W\cot(\gamma_n W)=-B_2$
*Y*21	$2/W$	$(2n-1)\pi/(2W)$
*Y*22	$\frac{2}{W}$; $\gamma_n\neq 0$ $\frac{1}{W}$; $\gamma_n=0$	$n\pi/W$; $n=0,1,2,\ldots$
*Y*23, *Y*24, *Y*25[a]	$2\phi_{2n}/W$	$\gamma_n W\tan(\gamma_n W)=B_2$
*Y*31, *Y*41, Y51[a]	$2\phi_{1n}/W$	$\gamma_n W\cot(\gamma_n W)=-B_1$
*Y*32, *Y*42, *Y*52[a]	$2\phi_{1n}/W$	$\gamma_n W\tan(\gamma_n W)=B_1$
*Y*33, *Y*34, *Y*35[b] *Y*43, *Y*44, *Y*45[b] *Y*53, *Y*54, *Y*55[b]	$2\Phi_n/W$	$\tan(\gamma_n W)=\frac{\gamma_n W(B_1+B_2)}{(\gamma_n W)^2-B_1B_2}$

[a]$\phi_{in}=[(\gamma_n W)^2+B_i^2]\div[(\gamma_n W)^2+B_i^2+B_i]$
[b]$\Phi_n=\phi_{2n}\div[(\gamma_n W)^2+B_1^2+B_1\phi_{2n}]$

5.2 Kernel Functions. With the above choices for $Y_n(x)$ and $N(\lambda_n)$ the kernel function $P(x,x')$ must satisfy

$$\frac{d^2P}{dx^2} - \sigma^2 P = -\frac{1}{\alpha}\delta(x-x') \tag{11}$$

Here function P has units ($s\,m^{-1}$) and parameter $\sigma^2=\gamma_n^2+j\omega/\alpha$ has units, m^{-1}. The solution for P may be found using two solutions of the homogeneous equation that satisfy the boundary conditions and are joined appropriately at $x=x'$ (see, for example, [21]). The kernel functions are given by

$$P(x,x',\sigma) = \frac{S_2^-(S_1^- e^{-\sigma(2L-|x-x'|)} + S_1^+ e^{-\sigma(2L-x-x')})}{2\alpha\sigma(S_1^+S_2^+ - S_1^-S_2^- e^{-2\sigma L})} + \frac{S_2^+(S_1^+ e^{-\sigma(|x-x'|)} + S_1^- e^{-\sigma(x+x')})}{2\alpha\sigma(S_1^+S_2^+ - S_1^-S_2^- e^{-2\sigma L})} \tag{12}$$

where the subscripts 1 and 2 represent the two boundaries at the smallest and largest x values, respectively. Coefficients S_M^+ and S_M^- depend on the boundary conditions on side M and are given by

$$S_M^+ = \begin{cases} 1 & \text{if side } M \text{ is type 0, type 1, or type 2} \\ k\sigma+\lambda_M & \text{if side } M \text{ is type 3, 4, or 5} \end{cases}$$

$$S_M^- = \begin{cases} 0 & \text{if side } M \text{ is type 0} \\ -1 & \text{if side } M \text{ is type 1} \\ 1 & \text{if side } M \text{ is type 2} \\ k\sigma-\lambda_M & \text{if side } M \text{ is type 3, 4, or 5} \end{cases}$$

The derivation of the kernel function given in Eq. (12) parallels that for steady-state GF given elsewhere [22]; however, in the present work σ is complex. The special case $\omega=0$, steady state has been treated previously for rectangles [23] and slabs [24].

5.3 Alternate Forms of GF. Although the GF is the unique solution to Eq. (7), for many geometries there exist alternate forms for the GF. These alternate forms have a very important role in numerical evaluation of the GF and the temperatures constructed from them. Specifically, the alternate GF can be used for verification that computed numerical values are correct. This usage of the word "verification" is somewhat similar to Roach [25] who discusses quantifying the error in a finite-element code by comparison with analytical solutions. In the present usage, verification is a comparison between two computer codes for numerical evaluation of alternate forms of the same analytical solution. Here the primary goal is improving one's confidence in the results,

rather than quantifying the error.

5.3.1 Alternate GF for Rectangles. In the rectangle an alternate series for the GF may be found by placing the kernel functions in the y direction and the eigenfunctions in the x direction. The alternate GF is important because at a point in the rectangle where one series converges slowly, the other series converges rapidly, and vice versa. In previous work with steady temperature, we have shown that there are locations in the domain at which the slowly converging series requires thousands of times more terms than the rapidly converging series [22,23]. A double-sum form of the GF may also be found from Fourier expansions along both x and y, however it generally converges very slowly and should not be used when a single-sum form is available.

5.3.2 Alternate GF for Slab Bodies. An alternate GF for slab bodies may be found with a spatial Fourier transform. Consider slab bodies described by cases $X00YIJ$ for which $I, J=1, 2, 3, 4,$ or 5. The solution will be found with a spatial Fourier transform defined by the following transform pair

$$\overline{G}(\beta) = \int_{-\infty}^{\infty} G(x) e^{-j\beta x} dx \tag{13}$$

$$G(x) = \frac{1}{2\pi} \int_{-\infty}^{\infty} \overline{G}(\beta) e^{j\beta x} d\beta \tag{14}$$

Note that variable x' has been suppressed by a change of variable, replacing $(x-x')$ by x, which is allowed under Eq. (7) which defines G. Apply the above transform to Eqs. (7) and (8) to obtain

$$\frac{\partial \overline{G}^2}{\partial y^2} - \nu^2 \overline{G} = -\frac{1}{\alpha} \delta(y - y') \tag{15}$$

$$k_i \frac{\partial \overline{G}}{\partial n_i} + \lambda_i \overline{G} = 0 \quad \text{at boundary } i \tag{16}$$

$$\text{where} \quad \nu^2 = \beta^2 + j\omega/\alpha \tag{17}$$

$$\lambda = h_i + j\omega(\rho c b)_i \tag{18}$$

Equation (15) is similar to Eq. (11) which defines the kernel function, so the solution for $\overline{G}$ is given by the kernel function from Eq. (12) with parameter σ replaced by ν and x replaced by y. That is, $\overline{G}(\beta, y, y', \omega) = P(y, y', \nu)$. Finally, the GF may be formally stated in x space by use of the inverse transform

$$G(x, y, \omega | x', y') = \frac{1}{2\pi} \int_{-\infty}^{\infty} P(y, y', \nu) e^{j\beta(x-x')} d\beta \tag{19}$$

Here variable x' has been recovered by reversing the earlier change of variable and replacing x by $(x-x')$. In general, the inverse-transform integral must be evaluated numerically, which is possible because the integrand approaches zero as $\beta \to \pm\infty$.

6 GF for Infinite and Semi-infinite Bodies

The GFs for infinite and semi-infinite bodies are found in the same manner as the alternate GF discussed above for the slab body. For cases $X00YI0$ for $I=0, 1, 2, 3, 4$ or 5, the kernel function P given in Eq. (12) may be simplified by taking $S_2^- = 0$ and $S_2^+ = 1$. Then the GF for infinite and semi-infinite bodies may be written

$$G(x, y, \omega | x', y') = \frac{1}{2\pi} \int_{-\infty}^{\infty} \frac{e^{j\beta(x-x')}}{2\alpha\nu} [e^{-\nu|y-y'|} + D e^{-\nu(y+y')}] d\beta$$

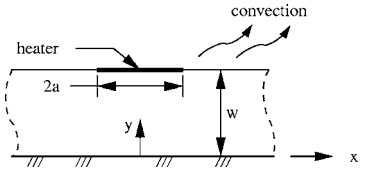

Fig. 2 Slab heated over a small area and cooled by convection

$$\text{where} \quad D = \begin{cases} 0 & \text{(infinite body)} \\ -1 & \text{(type 1 at } y=0\text{)} \\ +1 & \text{(type 2 at } y=0\text{)} \\ (k\nu - \lambda)/(k\nu + \lambda) & \text{(type 3, 4, or 5)} \end{cases} \tag{20}$$

For some cases the β integral is known in closed form. For cases $X00Y00$, $X00Y10$, and $X00Y20$, the GF may be written [18]

$$G(x, y, \omega | x', y') = \frac{1}{2\pi\alpha} \Big[K_0\Big(\nu\sqrt{(x-x')^2 + (y-y')^2}\Big) + D K_0\Big(\nu\sqrt{(x+x')^2 + (y+y')^2}\Big) \Big] \tag{21}$$

where K_0 is the modified Bessel function of order zero (with complex argument) and $D=0, -1,$ or 1 for cases $X00Y00$, $X00Y10$, and $X00Y20$, respectively.

7 Measurement Applications

In this section the temperature in bodies heated over a small region will be studied as simple models of devices used for measurement of thermal properties. For example, in the 3-omega method, a thin metal strip is plated on a solid surface and suitable electronics are used to introduce heat in a steady-periodic fashion. The thermal response is measured on the metal strip or at other locations on the solid surface [10]. As another example, in photothermal methods, a sample is heated by a periodically modulated laser beam and the thermal response is measured by optical or acoustic methods [7,8,14].

Generally thermal properties are measured indirectly, through a type of inverse problem, in which the thermal properties are deduced by a systematic comparison between the experimental data (such as temperature) and a thermal model. The thermal model is the subject of this discussion. The inverse problem, although an important part of the measurement process, is beyond the scope of this paper. For a discussion of inverse methods associated with thermal properties, see [6,26]. Next, numerical examples are given of thermal models appropriate for measurement applications constructed with two-dimensional steady-periodic GFs.

7.1 Slab Heated Over a Small Region. In this example a slab body is heated over a small region and cooled by convection on one side. The other surface of the body is insulated. The GF number for this case is $X00Y23$ and the geometry is shown in Fig. 2. The temperature is formally given by Eq. (6) with volume heating

$$T(x, y, \omega) = \frac{\alpha}{k} \int \int g(x', y') G_{X00Y23}(x, x', y, y', \omega) dx' dy' \tag{22}$$

The heated region is of infinitesimal thickness along y and is piecewise constant along x, described by $g(x', y') = q(x')\delta(y' - W)$ where

$$q(x') = \begin{cases} q_0; & |x'| < a \\ 0; & |x'| > a \end{cases}$$

This heating function could represent an electrically heated metal film with negligible thermal mass. Substitute the above heating function into the temperature expression, Eq. (22), to obtain

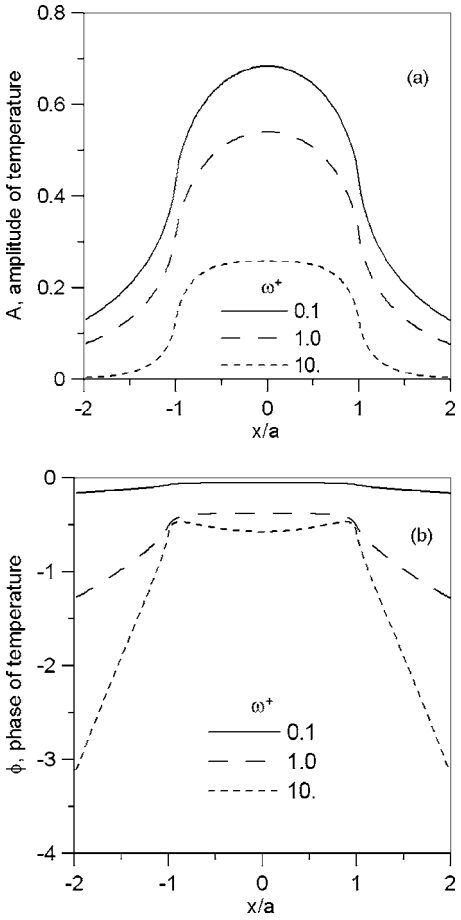

Fig. 3 Amplitude (*a*) and phase (*b*) of the temperature on the heated surface of a slab with $B_a=1$ and $W/a=1$ for three heating frequencies

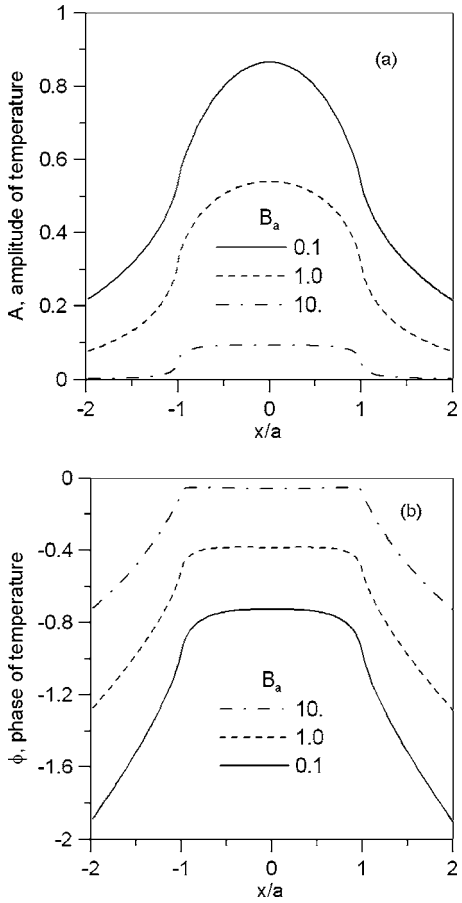

Fig. 4 Amplitude (*a*) and phase (*b*) of the temperature on the heated surface of a slab with heating frequency $\omega^+=1$ and $W/a=1$ for three Biot values

$$T(x,y,\omega)=\frac{\alpha}{k}\int_{-a}^{a} q_0 G_{X00Y23}(x,x',y,y'=W,\omega)dx' \qquad (23)$$

Note that the integral on y' has been stripped away by the Dirac delta function. The series form of the GF, Eq. (9), will be used to find the temperature. Substitute the appropriate eigenfunction from Table 2, norm from Table 3, and kernel function from Eq. (12) to obtain

$$T(x,y,\omega)=\frac{\alpha q_0}{k}\sum_{n=0}^{\infty}\frac{\cos(\gamma_n W)\cos(\gamma_n y)}{N_y}\int_{-a}^{a}\frac{e^{-\sigma|x-x'|}}{2\sigma\alpha}dx' \qquad (24)$$

$$\text{where}\quad N_y^{-1}=\frac{2}{W}\frac{\gamma_n^2W^2+(B_2W/a)^2}{\gamma_n^2W^2+(B_2W/a)^2+B_2W/a} \qquad (25)$$

Note that the integral on x' may be carried out in closed form.

Next, results are presented for the amplitude and phase of the dimensionless temperature on the $y=W$ surface of the slab. The amplitude of the temperature A, and phase of temperature ϕ, are computed as follows

$$A=[T\cdot T^*]^{1/2} \qquad (26)$$

$$\phi=\tan^{-1}[\text{Imag}(T)/\text{Real}(T)] \qquad (27)$$

where "Imag" and "Real" are the imaginary and real parts of the (complex) temperature, respectively. The following dimensionless variables are used for reporting results: for temperature, $T^+=Tk/(q_0a)$; for geometry, W/a; for convection, Biot number $B_a=ha/k$; and for frequency $\omega^+=\omega a^2/\alpha$. Figure 3 shows results for the surface temperature under conditions $B_a=1$ and $W/a=1$ for various values of the frequency ω^+. As the frequency increases the temperature amplitude decreases and the phase becomes more negative. Also for higher frequency a smaller region of the surface is participating in the periodic temperature variations. Figure 4 shows results for $\omega^+=1$, $W/a=1$ for several values of the Biot number, B_a, which controls convection cooling. At higher Biot number the amplitude decreases (convection cools the body) but the phase moves closer to zero. This is because with vigorous convection there is a smaller volume of the body participating in the heat transfer, and the phase lag will be smaller when the thermal mass is smaller. Figure 5 shows results for $B_a=1$ and $\omega^+=1$ for several values of the slab thickness W/a. As the slab becomes thinner the temperature amplitude grows, but it is more closely confined to the heated region. This is because there is less area for heat conduction along the x coordinate. As the slab becomes thinner the phase in the heated region moves toward zero, again because a smaller thermal mass participates in the heat transfer.

The alternate GF was also used to find the temperature in this case. The alternate GF is given by Eqs. (19) and (12) with $S_1^+=S_1^-=1$, $S_2^+=k\nu+\lambda_2$, and $S_2^-=k\nu-\lambda_2$ as appropriate for case $X00Y23$. Then the GF, evaluated at $y'=y=W$, is given by

$$G_{X00Y23}(x,0|x',0,\omega)=\frac{1}{2\pi}\int_{-\infty}^{\infty}\frac{e^{-j\beta(x-x')}W(1-e^{-2\nu W})d\beta}{\alpha[\nu W+B_2-(\nu W-B_2)e^{-2\nu W}]} \qquad (28)$$

The temperature is found by replacing the above GF into Eq. (23), to give

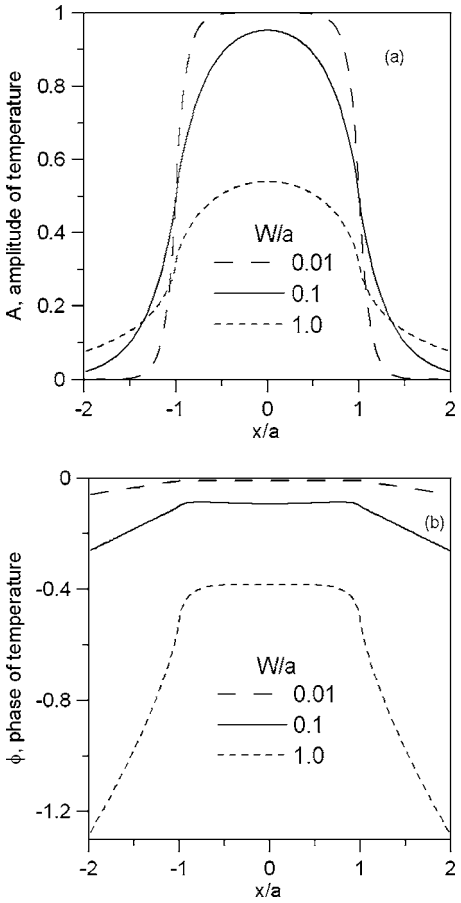

Fig. 5 Amplitude (*a*) and phase (*b*) of the temperature on the heated surface of a slab with B_a=1 and ω^+=1 for three slab thicknesses

$$T(x,y,\omega)=\frac{q_0W}{k}\int_{-\infty}^{\infty}\frac{e^{-j\beta(x-a)}-e^{-j\beta(x+a)}}{j\beta}\times\frac{(1-e^{-2\nu W})d\beta}{[\nu W+B_2-(\nu W-B_2)e^{-2\nu W}]} \tag{29}$$

Note that the integral over x' has been carried out in closed form, but the remaining integral on β must be carried out numerically. A Romberg integration scheme was used here. In a comparison with the series form of the temperature, Eq. (24), it was found that the above integral form required much more computer time for convergence than for the series form. Because of this, the integral form, Eq. (29), was primarily used for checking that the two forms produced plots in reasonable agreement. Agreement to three decimal places was used for this purpose. Higher-accuracy agreement could have been sought by tightening the convergence criteria, however this calculation was not attempted.

7.2 Thin Film on a Thick Substrate. Consider a thick substrate with properties k, ρc which is coated with a thin surface film with high conductivity ($k_1 \gg k$) and with volume thermal capacity $(\rho c)_1$. The surface film is in perfect thermal contact with the substrate. There is a strip heater and convection cooling similar to the previous example. Refer to Fig. 6. The GF needed for this case has number $X00Y50$.

The temperatures in the substrate may be formally stated with the GF solution equation given in Eq. (6)

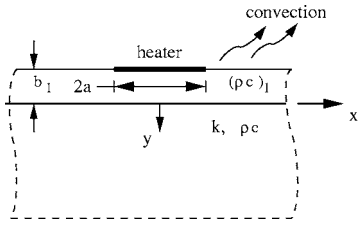

Fig. 6 Thin film on a thick substrate, heated over a small area and cooled by convection

$$T(x,y,\omega)=\frac{\alpha}{k}\int_{-\infty}^{\infty}q(x')G_{X00Y50}(x,y,\omega|x',y'=0)dx' \tag{30}$$

where $q(x')$ is the heat distribution introduced at $y=0$. The GF for this case, given in Eq. (20), contains a β integral that in general must be carried out with numerical quadrature. One approach to evaluating the above temperature would be to find G numerically and then evaluate the integral on x' numerically. A better approach is to examine the temperature in β space where the x' integral can be evaluated in closed form. Specifically, perform a spatial Fourier transform on Eq. (30) according to Eq. (13), and apply the convolution rule

$$\overline{T}(\beta,y,\omega)=\frac{\alpha}{k}\overline{q}(\beta)\overline{G}_{X00Y50}(\beta,y,y'=0,\omega) \tag{31}$$

In this approach the x' integral is removed by the Fourier transform. The β-space GF, $\overline{G}$, has been discussed earlier. Function $\overline{q}$ must be found from the spatial distribution of heating and the Fourier transform. For the strip heater with piecewise-constant heating over $(-a<x<a)$, function $\overline{q}$ is given by

$$\overline{q}(\beta)=q_0\int_{-a}^{a}e^{-j\beta x}dx=q_0\frac{e^{j\beta a}-e^{-j\beta a}}{j\beta} \tag{32}$$

Function $\overline{q}$ can also be found in closed form for a variety of other heating distributions (Gaussian, point source, etc.). Then, the temperature in real space is given by Eq. (31) combined with the transform-inversion integral

$$T(x,y,\omega)=\frac{1}{2\pi}\int_{-\infty}^{\infty}\overline{T}(\beta,y,\omega)e^{j\beta x}d\beta \tag{33}$$

7.2.1 Average Temperature on the Heater. Rather than show the spatial distribution of temperature, which has many of the same trends as the previous example, numerical results are presented below for the average temperature on the heater.

The average temperature on the heater is of great importance for thermal-property measurements for which a metal film is used simultaneously as a heater and as a temperature sensor. To find the spatial average, evaluate the above temperature expression on the body surface ($y=0$), integrate over the heated region, and divide by the length of the heated region

$$T_{av}(\omega)=\frac{1}{2\pi}\int_{-\infty}^{\infty}\overline{T}(\beta,y=0,\omega)\left[\frac{1}{2a}\int_{-a}^{a}e^{j\beta x}dx\right]d\beta \tag{34}$$

Note that the spatial integral, shown in brackets in the above expression, may be evaluated in closed form. Now use $\overline{T}$ from Eq. (31), $\overline{q}$ from Eq. (32), and $\overline{G}$ from Eq. (20) to find

$$T_{av}(\omega)=\frac{1}{4\pi}\frac{q_oa}{k}\int_{-\infty}^{\infty}\frac{(e^{j\beta a}-e^{-j\beta a})^2}{(j\beta a)^2}\frac{ad\beta}{(\nu a+\lambda a/k)} \tag{35}$$

Although numerical quadrature for the transform-inversion integral cannot be avoided, with this approach quadrature is only

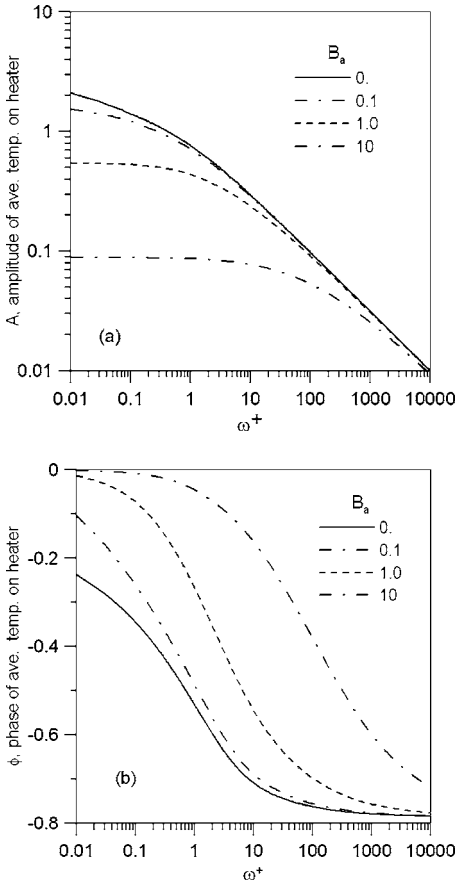

Fig. 7 Amplitude (*a*) and phase (*b*) of the spatial average temperature on the heater for a thick substrate with no surface film as a function of frequency for three convection values

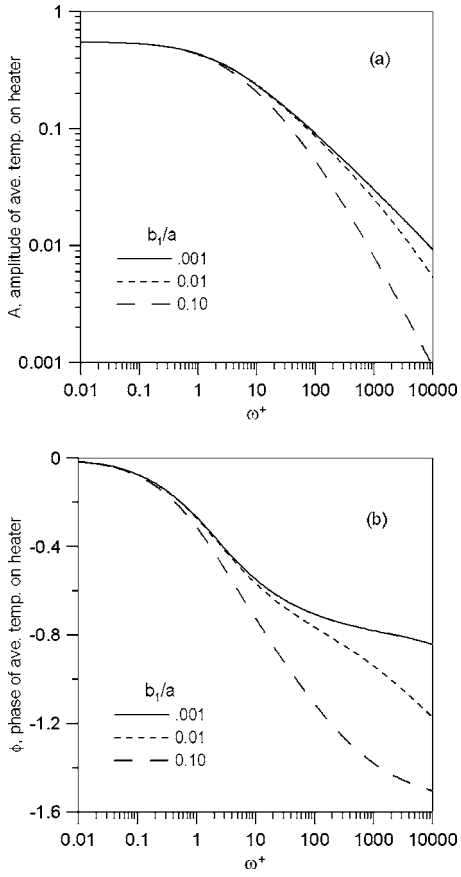

Fig. 8 Amplitude (*a*) and phase (*b*) of the spatial average temperature on the heater as a function of frequency at B_a=1 for various thicknesses of films on a large substrate. For the films, $(\rho c)_1/(\rho c)$=1.

needed once.

Next numerical results will be discussed, beginning with the semi-infinite substrate with no surface film (b_1=0). Figure 7 shows the dimensionless spatial-average temperature (amplitude and phase) on the heater over a wide range of frequency values for values of the surface convection. The highest amplitude occurs for Biot = 0 representing no convection cooling (insulated surface). As the convection value increases the amplitude falls and the phase moves closer to zero. These trends agree with those discussed in the previous example.

Figure 8 shows the effect of adding a high-conductivity surface film, with $(\rho c)_1/(\rho c)$=1.0, to the substrate. All results shown in Fig. 8 are at Biot=1.0 and the heating conditions are the same as those shown in Fig. 7. Figure 8 shows that the surface film has an increasing effect as the film thickness increases and as the frequency increases. A comment is needed on the frequency behavior of the results with the surface film. There is a maximum frequency beyond which the thin-film assumption breaks down, determined approximately when $\omega b_1^2/\alpha \approx 1$ when the thermal penetration into the substrate becomes small enough to approach the thickness of the surface film. This effect may explain the shape of the phase curves in Fig. 8 at higher frequencies. The effect is more pronounced as b_1 becomes larger.

Results for several other Biot values were also explored, however, as the trends are identical to those shown in Fig. 8, results for Biot $\neq$ 1 are not shown to save space.

7.2.2 Computer Issues. About 2 min of computer time was required to compute the 300 temperature values plotted for each curve shown in Figs. 7 and 8. Computations were carried out on a Sun Blade 2000 with dual 900 MHz processors running the Solaris operating system. The calculations were coded in Fortran 77 with variables of type double-precision complex.

Numerical integration for the inverse transform from β space to x space was carried out efficiently with the recognition that the integrand contains an infinite number of zero crossings along the β axis at regular intervals of 2π, and that the amplitude decays monotonically as $\beta \rightarrow \pm\infty$. Then, the integration over domain $(-\infty < \beta < \infty)$ was carried out by a series of integrations over subdomains of size 2π beginning at β=0. Within each subdomain, a Romberg integration scheme converged rapidly. By examining the relative contribution of successive subdomains, the infinite domain was truncated while retaining control over the numerical precision of the result. The numerical-integration routine for the inverse transform was checked by computing case *X*00*Y*20 based on Eq. (20), and then comparing with the closed-form expression given in Eq. (21). Six-digit agreement was obtained.

8 Conclusions

Verification of numerical results is an important part of any numerical calculation. The Green's function method presented here provides two distinct opportunities for verification. First, a variety of Green's functions are presented for closely related geometries, which allow for the construction of useful limiting cases. For example, case *X*00*Y*30 was used to check case *X*00*Y*32. Second, the alternate Green's functions, given here for rectangles and slabs, may be used to construct alternate expressions for the same temperature. These alternate temperature expressions, although they represent the same unique solution, have different

computational behaviors. They may be checked, one against the other, to ensure that numerical values may be found not only with high precision, but with high confidence that the results are correct.

In this paper a variety of Green's function solutions are given for steady-periodic heat conduction in two-dimensional bodies in rectangular coordinates. Five types of boundary conditions are treated. Numerical results are presented for two geometries involving bodies heated over a small region related to thermal-property measurements. Because the method is computationally efficient, results were reported over 6 decades of frequency under several different conditions.

Nomenclature

a = half-width of heated region (m)
A = temperature amplitude, Eq. (26)
B_a = Biot number, ha/k
B_i = Biot number, $h_i W/k$, see Table 3.
b_i = film thickness on boundary i (m)
c = specific heat (J kg^{-1} K^{-1})
D = Coefficient in Eq. (20)
f = known effect at boundary i
G = steady-periodic Green's function (s m^{-2})
g = internal heating at frequency ω (W m^{-3})
h = heat transfer coefficient, (W m^{-2} K^{-1})
j = imaginary number, $\sqrt{-1}$
K_0 = modified Bessel function, order zero
k = thermal conductivity (W m^{-1} K^{-1})
L = length of domain in x direction (m)
n_i = outward-facing unit normal vector on boundary i
N_y = norm, Eq. (9) (m)
P = kernel function, Eq. (12) (s m^1)
q = steady-periodic heat flux (W m^{-2})
S_M = coefficient for kernel function in Eq. (12)
ds_i = dx_i or dy_i depending on boundary i (m)
$\underline{T}$ = steady-periodic temperature (K)
$\overline{T}$ = β-space temperature (K m)
T^+ = $Tk/(q_0 a)$
t = time (s)
W = width of domain in y direction (m)
Y_n = eigenfunction, Eq. (10)
Y_n^* = complex conjugate of eigenfunction

Greek

α = thermal diffusivity (m^2 s^{-1})
β = wave number, Eq. (14) (m^{-1})
γ = eigenvalue, Table 3 (m^{-1})
δ = Dirac delta function
λ = boundary parameter, Eq. (18)
ν = $(\beta^2 + j\omega/\alpha)^{1/2}$ (m^{-1})
ρ = density (kg m^{-3})
σ = $(\gamma_n^2 + j\omega/\alpha)^{1/2}$ (m^{-1})
ϕ = phase, Eq. (27)
ω = frequency (rad s^{-1})
Ω = domain

References

[1] Carslaw, H. S., and Jaeger, J. C., 1959, *Conduction of Heat in Solids*, Oxford University Press, Oxford, UK, pp. 108,111.
[2] Gustafsson, S. E., 1979, "Thermal Properties of Thin Insulating Layers Using Pulse Transient Hot Strip Measurements," J. Phys. D, **12**, pp. 1411–1421.
[3] English, A. T., Miller, G. L., Robinson, D. A. H., Dodd, L. V., and Chynoweth, T., 1978, "Pulse Nonlinearity Measurements on Thin Conducting Films," J. Appl. Phys., **49**, pp. 717–722.
[4] Gustafsson, S. E., and Karawacki, E., 1983, "Transient Hot-Strip Probe for Measuring Thermal Properties of Insulating Solids and Liquids," Rev. Sci. Instrum., **54**, pp. 744–747.
[5] Zhong, Q. Y., Favro, L. D., and Thomas, R. L., 2000, "Thermal Wave Reflections of a Pulsed Stripe Heat Source From a Plane Boundary," J. Appl. Phys., **87**, pp. 3999–4004.
[6] Haji-Sheikh, A., Hong, Y. S., You, S. M., and Beck, J. V., 1998, "Sensitivity Analysis for Thermophysical Property Measurements Using the Periodic Method," ASME J. Heat Transfer, **120**, pp. 568–576.
[7] McGahan, W. A., and Cole, K. D., 1992, "Solution of the Heat Conduction Equation in Multilayers for Photothermal Deflection Experiments," J. Appl. Phys., **72**, pp. 1362–1373.
[8] Hu, H., Wang, X., and Xu, X., 1999, "Generalized Theory of the Photoacoustic Effect in a Layered Material," J. Appl. Phys., **86**, pp. 3953–3958.
[9] Aviles-Ramos, C., Haji-Sheikh, A., Beck, J. V., and Dowding, K. J., 2001, "Estimation of Thermophysical Properties by the Spectral Method–Development and Evaluation," ASME J. Heat Transfer, **123**, pp. 24–30.
[10] Cahill, D. G., 1990, "Thermal Conductivity Measurement From 30 to 750 K: the 3ω Method," Rev. Sci. Instrum., **61**, pp. 802–808.
[11] Kim, J. H., Feldman, A., and Novotny, D., 1999, "Application of the Three Omega Thermal Conductivity Measurement Method to a Film on a Substrate of Finite Thickness," J. Appl. Phys., **86**, pp. 3959–3963.
[12] Borca-Tasciuc, T., Kumar, A. R., and Chen, G., 2001, "Data Reduction in 3ω Method for Thin-Film Thermal Conductivity Determination," Rev. Sci. Instrum., **72**, pp. 2139–2147.
[13] Cole, K. D., 2004, "Analysis of Photothermal Characterization of Layered Materials–Design of Optimal Experiments," Int. J. Thermophys., **25**, pp. 1567–1584.
[14] Cole, K. D., and McGahan, W. A., 1993, "Theory of Multilayers Heated by Laser Absorption," ASME J. Heat Transfer, **115**, pp. 767–771.
[15] Beck, J. V., Cole, K. D., Haji-Sheikh, A., and Litkouhi, B., 1992, *Heat Conduction Using Green's Functions*, Hemisphere, New York, Chap. 2, pp. 40–43.
[16] Duffy, D. G., 2001, *Green's Functions With Applications*, Chapman and Hall/CRC, Boca Raton, FL.
[17] Sheremet, V. D., 2002, *Handbook of Green's Functions and Matrices*, WIT, Southhampton, UK.
[18] Mandelis, A., 2001, *Diffusion-Wave Fields, Mathematical Methods and Green's Functions*, Springer, New York, pp. 2, 3, and 231.
[19] Cole, K. D., Green's Function Library, www.greensfunction.unl.edu
[20] Haji-Shiekh, A., and Beck, J. V., 2002, "Temperature Solution in Multi-Dimensional Multi-Layer Bodies," Int. J. Heat Mass Transfer, **45**, pp. 1865–1877.
[21] Stakgold, I., 1967, *Boundary Value Problems of Mathematical Physics*, MacMillian, New York, Chap. 1.
[22] Crittenden, P. E., and Cole, K. D., 2002, "Fast-Converging Steady-State Heat Conduction in a Rectangular Parallelepiped," Int. J. Heat Mass Transfer, **45**, pp. 3585–3596.
[23] Cole, K. D., and Yen, D. H. Y., 2001, "Green's Functions, Temperature, and Heat Flux in the Rectangle," Int. J. Heat Mass Transfer, **44**, pp. 3883–3894.
[24] Cole, K. D., and Yen, D. H. Y., 2001, "Influence Functions for the Infinite and Semi-Infinite Strip," J. Thermophys. Heat Transfer, **15**, pp. 431–438.
[25] Roach, P. J., 1998, "Verification and Validation in Computational Science and Engineering," *Hermosa*, Albuquerque, NM, p. 23.
[26] Beck, J. V., and Arnold, K. J., 1977, *Parameter Estimation in Engineering and Science*, Wiley, New York.